

Importance Sampling CAMs for Weakly-Supervised Segmentation with Highly Accurate Contours

Arvi Jonnarth, Michael Felsberg, *Senior Member, IEEE*, and Yushan Zhang

Abstract—Classification networks have been used in weakly-supervised semantic segmentation (WSSS) to segment objects by means of class activation maps (CAMs). However, without pixel-level annotations, they are known to (1) mainly focus on discriminative regions, and (2) to produce diffuse CAMs without well-defined prediction contours. In this work, we alleviate both problems by improving CAM learning. First, we incorporate importance sampling based on the class-wise probability mass function induced by the CAMs to produce stochastic image-level class predictions. This results in segmentations that cover a larger extent of the objects, as shown in our empirical studies. Second, we formulate a feature similarity loss term, which further improves the alignment of predicted contours with edges in the image. Furthermore, we shed new light onto the problem of WSSS by measuring the contour F-score as a complement to the common area mIoU metric. We show that our method significantly outperforms previous methods in terms of contour quality, while matching state-of-the-art on region similarity.

Index Terms—Weak supervision, semantic segmentation, importance sampling, feature similarity, class activation maps

1 INTRODUCTION

THE advancements of deep learning methods in recent years have had a major impact on many computer vision tasks, with no exception for semantic segmentation. The ability to automatically segment images has been found useful in many applications, including autonomous driving [1], video surveillance [2], and medical image analysis [3]. Fully-supervised segmentation frameworks have achieved remarkable results by utilizing large datasets of pixel-wise annotated images. However, these annotations require a significant manual labelling effort, which increases with the dataset size. Image-level weakly-supervised semantic segmentation (WSSS) aims to alleviate the labelling effort, where, instead of requiring human-annotated pixel-wise segmentation masks, the only source of supervision are cheap image-level classification labels. This opens the possibility to train segmentation models on existing large-scale datasets where pixel-level labels are non-existent and infeasible to acquire.

A common approach to WSSS is to first train a classification network with global average pooling (GAP) to produce class activation maps (CAMs) [5]. The CAMs are used to generate pseudo-labels for supervising the final segmentation network [4], [6], [7]. However, classification networks are known to (1) mainly focus on discriminative regions as opposed to the whole extent of objects, and

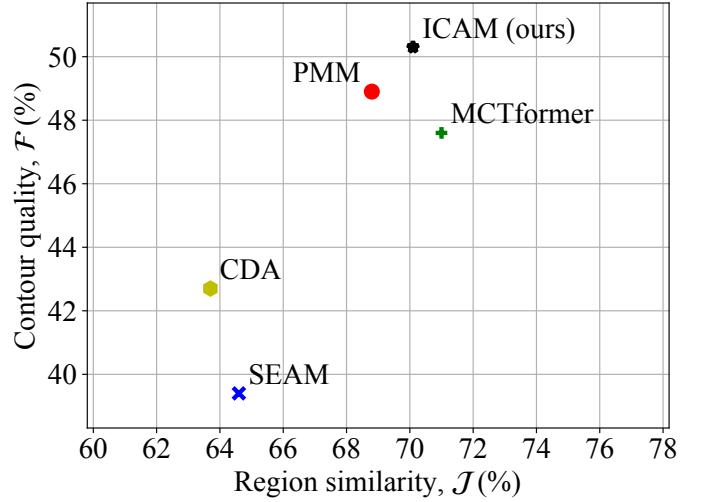


Fig. 1. Region similarity versus contour quality compared to previous methods, reproduced from original implementations. Our method achieves the highest contour quality while attaining a competitive region similarity.

(2) to produce overly smooth CAMs without well-defined prediction contours [5], [6], [7]. In this work, we improve the CAMs in these two aspects. We substitute GAP with *importance sampling* by sampling from the class-wise probability mass function induced by the CAMs to produce stochastic image-level class predictions during training. This leads to segmentations that cover a larger extent of the objects, and not only the discriminative regions. This approach is motivated by the effectiveness of similar stochastic mechanisms, such as particle filters [8], random sample consensus [9], and the saccadic movement of eyes [10].

Furthermore, we notice a discrepancy in the evaluation

- A. Jonnarth is with the Department of Electrical Engineering, Linköping University, Sweden, and Husqvarna Group, Huskvarna, Sweden.
E-mail: arvi.jonnarth@liu.se
- M. Felsberg is with the Department of Electrical Engineering, Linköping University, Sweden, and co-affiliated with the University of KwaZulu-Natal, Durban, South Africa.
E-mail: michael.felsberg@liu.se
- Y. Zhang is with the Department of Electrical Engineering, Linköping University, Sweden.
E-mail: yushan.zhang@liu.se

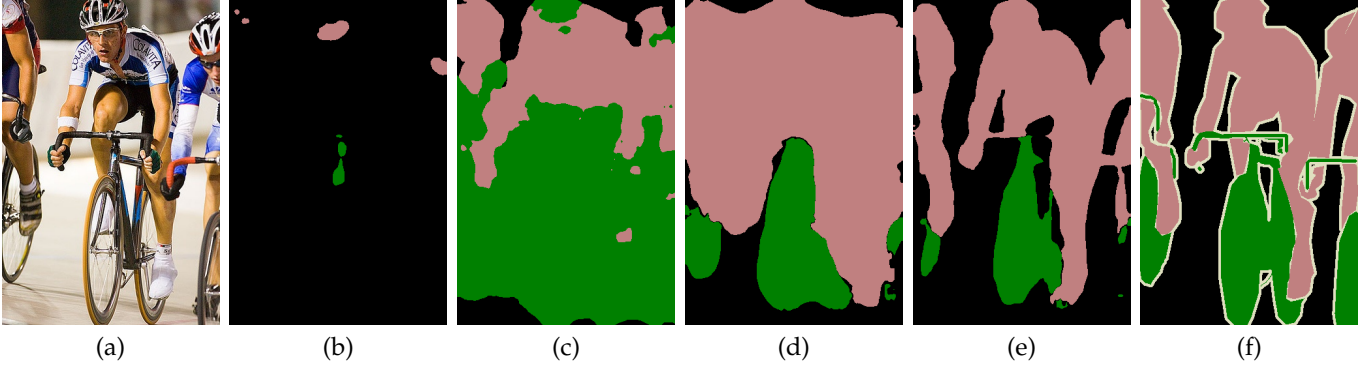


Fig. 2. CAM comparison. (a) Input image. Pseudo-labels with (b) max pooling, (c) average pooling (SEAM [4]) (d) importance sampling (ours), and (e) importance sampling and feature similarity loss (ours). (f) ground truth.

in WSSS benchmarks compared to related computer vision tasks, such as video object segmentation (VOS). In WSSS benchmarks, only region similarity is evaluated using the mean intersection over union (mIoU) based on the area of segmentation masks. However, a complementary aspect not considered is the contour quality, which might be equally or even more important depending on the application. For example, contours contribute more to the perceived visual quality [11], and bear more weight in cases where the segmentations are displayed to a human, such as in virtual green-screen applications. We suggest to use the contour F-score to evaluate the contour quality of WSSS methods, similar to how VOS methods are evaluated in the well-established DAVIS benchmark [12]. We find that current state-of-the-art WSSS methods lack in this regard. Thus, we aim to develop a method that improves upon the contour quality, while keeping the high region similarity of previous works. We propose a new *feature similarity loss term* (FSL) which aims to match prediction contours with color edges in the image. This significantly improves the contour quality over previous methods, which is shown quantitatively in Figure 1, and visually illustrated in Figure 2. Compared to an early version of this method [13], we sample several pixels per class during importance sampling, incorporate GAP to implicitly alter the sampling distribution, and fix parameters in FSL instead of learning them during training. A code implementation is available at [github](https://github.com/arvijj/icam).¹ Our contributions can be summarized as follows:

- We propose to use *importance sampling* for pixel- to image-level aggregation in order to cover the whole extent of objects.
- We introduce a new *feature similarity loss term* for improving contours.
- We suggest to evaluate WSSS methods in terms of contour quality, in addition to region similarity, similar to related computer vision tasks, such as the DAVIS benchmark [12].
- Finally, we perform extensive experiments and ablations on the PASCAL VOC benchmark dataset to validate the effectiveness of our approach.

2 RELATED WORK

Weakly-supervised semantic segmentation has its background in several sub-fields, for which we describe the related work below. The sub-fields include different types of weak supervision, the learning of class activation maps, pixel-to-image aggregation, the use of feature similarities to refine segmentation predictions, as well as the implicit model distillation used in many WSSS methods.

Types of weak supervision. Depending on the application and available data, one might have access to different types of annotations. Therefore, it is of interest to find methods that can learn to segment images based on various types of weak supervision. Semantic segmentation networks have successfully been trained in the past without access to full annotations in the form of segmentation masks. This has been achieved by utilizing different types of weak labels during training, such as bounding boxes [14], [15], [16], scribbles [17], [18], points [19] and classification labels, in decreasing levels of supervision. Classification labels have been the most popular as they require the least amount of manual labelling effort, and it is clear that they can be gathered from any of the stronger label types. Classification labels have been used for learning CAMs [4], [7] and pixel affinities [6], constraining the neural network output [20], seeding, expanding and constraining the segmentation predictions [21], as well as using them in combination with saliency maps [22], all in order to increase the quality of the segmentation predictions. In this work, we focus on the lowest level of weak supervision, that is, image-level classification labels.

Class activation maps. Class activation maps [5], [23] have been used to visualize what part of the input a neural network uses to base its prediction on. CAMs are usually produced using GAP in the final layers, where class predictions are propagated into pixel space. Due to their ability to give an indication of the position and size of objects without ground-truth segmentation masks, they have been adapted in many WSSS methods. Ahn et al. [6] use CAMs as a starting point for predicting pixel affinities, which they use to produce better segmentation predictions. Wang et al. [4] improve the generation of CAMs with a siamese network architecture and equivariant regularization to further improve results. Oquab et al. [24] use global max-pooling to produce image-level class predictions during

1. <https://github.com/arvijj/icam>

training, where they use the activation maps for object localization. In this work, we choose a slightly different approach to previous methods by using random sampling instead of pooling to produce classification predictions. We show that this approach leads to better CAMs in terms of activating over the entire extent of objects as opposed to focusing on small discriminative regions. Therefore, it is well suited for the task of semantic segmentation. Lee et al. [7] also use stochasticity for improving CAMs, where they use spatial dropout for hidden unit selection in order to produce multiple localization maps during both training and inference. Our approach differs in two ways. First, we use a non-uniform sampling strategy based on the CAMs for sampling image-level classification predictions. Second, we only use it during training, thus employing a deterministic inference scheme.

Pixel-to-image aggregation. Advanced pooling strategies have been extensively studied in the past, and some have suggested to use activation ranking which shares some similarities with importance sampling. Kolesnikov & Lempert [21] introduce global weighted rank-pooling (GWRP) which aggregates the pixel-level activations by ranking them and assigning a weight based on the rank. Durand et al. [25] combine the highest and lowest activations to form their spatial pooling strategy. Our approach differs in that neither of the previous works perform sampling, while they both include an implicit object size prior defined by method-related parameters.

Prediction-propagation based on feature similarities. The concept of propagating a signal to spatial neighbours based on feature similarities has been studied in the past, whether it be by computing a weighted mean of nearby pixels for image denoising [26], or by letting the raw image features define the pair-wise potentials in a fully connected conditional random field (CRF) for propagating initial segmentation predictions iteratively [27]. Ahn et al. introduce an additional network for learning class-agnostic pixel affinities [6]. More recently, prediction propagation has been used in an attention-based WSSS approach where the CAM predictions are propagated to similar pixels based on deep features in order to improve segmentation results [4]. In this work, we propose to do this implicitly through a class-specific *feature similarity loss term* based on pixel and prediction similarities, which is minimized when the prediction contours of CAMs match the edges in the image.

Model distillation. Many state-of-the-art WSSS methods [4], [7], [28] implicitly take advantage of model distillation, by applying the two-stage framework of first generating pseudo-labels using a classification network, and subsequently training a segmentation network on the generated pseudo-labels in a fully supervised setting. As has been demonstrated in the past [29], [30], large ensembles of models can be distilled into a single model without a significant loss of performance by training the final model to predict the output of the ensemble. Recently, it has also been shown that only one model is sufficient to be used as the “ensemble” to gain better results compared to simply training the final model directly on the data [31]. This is referred to as self-distillation. In a sense, the two-stage framework in WSSS is a form of self-distillation, and we also take advantage of

this phenomenon by adapting the two stages in generating pseudo-labels for the final segmentation network.

3 APPROACH

In this section we describe our approach of training a network for predicting CAMs, and how we integrate our two main method contributions from Secs. 3.2 and 3.3 for improving them.

3.1 Computing CAMs

Let $a_\theta(x) \in [0, 1]^{W \times H \times K}$ denote a class activation map (CAM) which is a function of the input image x , and parameterized by θ , where W , H and K denote the width, height and number of classes (including background) respectively. Furthermore, let $s_\theta(x)_{ijk}$ represent the unnormalized logit of class k at the position indexed by i and j . Typically, this is the output of the last convolutional layer without activation function. If we model the class probabilities in each pixel as a normalized probability distribution we can estimate the probability that a pixel contains a certain class k using the softmax function as

$$a_\theta(x)_{ijk} := \Pr(z_{ij} = k|x) = \frac{e^{s_\theta(x)_{ijk}}}{\sum_{t=1}^K e^{s_\theta(x)_{ijt}}}, \quad (1)$$

where $z \in \mathbb{R}^{W \times H}$ is the ground-truth segmentation mask and z_{ij} is the class index present at the pixel indexed by i and j . $\Pr(z_{ij} = k|x)$ is the estimated probability that class k is present in pixel (i, j) in a given image x .

Since z is unknown in the weakly supervised setting, the pixel-wise class predictions need to be condensed into an image-level prediction. Commonly, global average pooling (GAP) on the unnormalized logits has been used in WSSS for this purpose [4], [6]. In this case the image-level probability that class k is present in the image is given by the logistic function

$$\hat{y}_k^{\text{GAP}} = \frac{e^{s_k}}{e^{s_k} + 1}, \quad (2)$$

and where the image-wide average of the logits is given by

$$s_k = \frac{1}{HW} \sum_{ij} s_\theta(x)_{ijk}. \quad (3)$$

However, when minimizing a classification loss in this case, every pixel contributes to the loss. Thus, if an image contains an object of class k , the loss encourages the model to classify every pixel as belonging to that class. This might lead to over-activation, blurry class activations and poorly defined prediction contours, see for example the result of a GAP-based method in Fig. 2c. Instead, we choose a different approach.

Assuming that, in order for an image to be classified as containing an object, it suffices that only one pixel contains that object, then we predict the probability $\Pr(k \in \{z_{ij}\}_{i=1, j=1}^{W, H} | x)$. We sample a single pixel per class based on the probabilities a_θ since this essentially translates to “if at least one pixel contains an object, the whole image contains this object”. The first obvious option is to apply global max pooling for this purpose, where the predicted image-level probabilities can be written as

$$\hat{y}_k^{\text{GMP}} := \Pr(k \in \{z_{ij}\}_{i=1, j=1}^{W, H} | x) = \max_{ij} a_\theta(x)_{ijk}. \quad (4)$$

A shortcoming of max pooling, however, is that it tends to activate over small discriminative regions and does not offer very useful segmentation predictions, even in cases where the classification prediction is correct. This can be observed in Fig. 2b. To improve the CAMs in this regard we use *importance sampling* to produce stochastic image-level class predictions during training.

3.2 Importance Sampling

As described in the previous section, global max pooling (GMP) tends to activate over small discriminative regions and does not leverage adequate segmentation predictions for pseudo-label generation. To solve this problem we introduce an additional image-level prediction by sampling one pixel for each class using the probability mass function induced by the class activation map a_θ . Let us define K probability mass functions, one for each class

$$p_k(I, J|x) = \Pr(I = i, J = j|x, k) = \frac{1}{Z_k(a)} a_\theta(x)_{ijk}, \quad (5)$$

where $Z_k(a) = \sum_{i=1}^W \sum_{j=1}^H a_\theta(x)_{ijk}$ is a normalizing constant. Now, we sample image coordinates for each class, which we use to extract the class activations. These activations are then interpreted as classification predictions

$$\tilde{y}_k = a_\theta(x)_{i\hat{j}k}, \quad (\hat{i}, \hat{j}) \sim p_k(I, J|x). \quad (6)$$

If the distributions p_k were uniform, this method would be similar to GAP since each pixel would have been given the same weight. Note also that in this case the distributions would not be conditioned on the input image x . However, in the case of the activation-based distributions in (5), the probability mass depends on the class activations, and pixels with higher activations are more likely to be sampled. Furthermore, pixels with zero activation for a certain class are never sampled and do not contribute to the classification loss term for that class. Note also that since we use softmax in (1), at least one class will have a non-zero probability in every pixel.

We can further compare GAP and importance sampling by considering the case of small objects. With GAP, in order for a model to perform a correct image-level prediction that an object is present in the image, it would have to output large positive logits at the few pixels resembling the object while outputting small negative logits at the majority of pixels not part of the object. Therefore, the model is not encouraged to predict the absence of objects with high certainty, a constraint not present for importance sampling. Essentially, we avoid the problem of GAP, that pixels, which are correctly classified as not containing an object, get reflected negatively on the loss in cases where the object is present somewhere else in the image.

If the distributions had instead been defined as the Kronecker delta function and equal to 1 at the maximum activation, we would get max pooling. Similar to max pooling, we choose one pixel to represent the image-level prediction for each class, but we choose them randomly based on the class activations. This allows the model to activate over the whole extent of objects and not only on the most discriminative regions.

Due to the nature of convolutional neural networks, they tend not to activate only at a specific pixel, but rather over a region of pixels, since the visual features are spatially correlated. Thus, for a model that under-activates, in the worst case we would sample pixels from a small region around discriminant features. Eventually, pixels at the prediction border would be sampled and the model would be encouraged to associate also these pixels with the object, thus covering a larger extent of it. Conversely, for a model that over-activates, pixels that do not correspond to object features would eventually be sampled. This behaviour is penalized in images where the feature is present but not the object. Thus, importance sampling encourages the model to activate only over the objects themselves.

The parameters θ can be found by minimizing the sum of K binary cross-entropy loss terms

$$\mathcal{L}_{ce}(y, \tilde{y}; \theta) = -\frac{1}{K} \sum_{k=1}^K y_k \log \tilde{y}_k + (1 - y_k) \log(1 - \tilde{y}_k), \quad (7)$$

where y_k is the image-level label for class k , which is equal to 1 if class k is present in the image and 0 otherwise. To understand how the behaviour shifts, we train our CAM network using a classification loss containing two cross-entropy terms, one for the prediction \hat{y} computed using either GMP or GAP, and one for the prediction \tilde{y} attained by random sampling according to (5) and (6). Our classification loss term is a convex combination of these two terms

$$\mathcal{L}_{cls}(y, \hat{y}, \tilde{y}) = (1 - \lambda) \mathcal{L}_{ce}(y, \hat{y}) + \lambda \mathcal{L}_{ce}(y, \tilde{y}), \quad (8)$$

where $\lambda \in [0, 1]$ is a parameter controlling the weight between the two cross-entropy terms. A value of $\lambda = 0$ corresponds to the case described in Sec. 3.1 with no importance sampling, and a value of $\lambda = 1$ corresponds to only using stochastic predictions during training. While the first cross-entropy term has been successful in classification tasks, it is unclear whether the first, second or a combination of the two is most suitable for weakly-supervised segmentation.

In our early experiments we observed that importance sampling improved the CAMs in terms of covering a larger extent of the objects, but the prediction borders did not align with their edges, see Fig. 2d. For this reason we introduce a *feature similarity loss term*, which aims to match the prediction contours with the edges of objects.

3.3 Feature Similarity Loss

Intuitively, similar pixels that are in close proximity have a high probability of being part of the same object. Additionally, if two nearby pixels are dissimilar, there is a chance that they belong to different classes and that the contour runs somewhere between them. Based on this rationale, we formulate a loss term which penalizes dissimilar predictions for nearby similar pixels. Furthermore, similar predictions are discouraged for nearby dissimilar pixels if their predictions are sufficiently dissimilar to begin with. In what follows, we formulate our feature similarity loss term as a function of the pixel-wise class predictions and features. Subsequently, we describe the intuition behind our formulation.

In the following equations we use a single index for the image coordinates in order to reduce notational clutter. First,

let us define a gating function $g(a_i, a_j) : \mathbb{R}^{2K} \rightarrow \mathbb{R}_+$ which computes the distance between the predictions a_i and a_j of the pixels i and j , as well as a function $f(d) : [0, 1] \rightarrow [-1, 1]$ which maps the dissimilarity $d(x_i, x_j) \in [0, 1]$ between the features x_i and x_j monotonically to $[-1, 1]$. Inspired by bilateral filtering [32], which considers both geometric and photometric similarity, we formulate the feature similarity loss term

$$\mathcal{L}_{fs}(a, x) = -\frac{1}{(HW)^2} \sum_{ij} w_{ij} g(a_i, a_j) f(d(x_i, x_j)), \quad (9)$$

where w_{ij} is a spatial weight which considers the distance between pixels i and j and is used to give a higher weight to pixel pairs which are close to each other. Note that a_i and x_i are vectors representing respectively the class probability distribution and image features for pixel i . Throughout our experiments we define the weights using a Gaussian neighbourhood

$$w_{ij} = \frac{1}{2\pi\sigma^2} \exp\left(-\frac{\|p_i - p_j\|_2^2}{2\sigma^2}\right), \quad (10)$$

where p_i and p_j are two-dimensional vectors containing the image coordinates of pixels i and j , and σ is the standard deviation of the Gaussian function to control the size of the considered pixel neighbourhood. Furthermore, we define the gating function g as the squared L^2 distance between the predictions

$$g(a_i, a_j) = \frac{1}{2} \|a_i - a_j\|_2^2, \quad (11)$$

and the function f as

$$f(d(x_i, x_j)) = \tanh\left(\mu + \log\left(\frac{d}{1-d}\right)\right), \quad (12)$$

where μ is a bias parameter. The logarithm in (12) computes the logit of the binary decision problem whether or not two pixels are (dis)similar. The tanh function then maps the logit with the added bias from \mathbb{R} onto the interval $[-1, 1]$. Thus, f takes the values -1 and $+1$ when pixels are similar ($d = 0$) and dissimilar ($d = 1$) respectively, and μ controls the cross-over point at which f changes sign.

For two similar pixels, we have $f < 0$ and get $\mathcal{L}_{fs} \geq 0$ since $g \geq 0$. \mathcal{L}_{fs} is thus minimized if g is minimized, i.e. if $a_i = a_j$. In the case of two dissimilar pixels on the other hand, i.e. if $f > 0$, we have $\mathcal{L}_{fs} \leq 0$, which is minimized if g is maximized, and occurs when a_i and a_j are opposite predictions, i.e. if they are two one-hot vectors predicting different classes. However, it is not always the case that two dissimilar pixels are part of different classes. For example, an object could contain some high-frequency texture or be made up of several parts with different visual appearance. However, since the gating function is chosen to be the squared L^2 distance, the gradient of \mathcal{L}_{fs} with respect to the predictions is proportional to the difference between the predictions, and equal to zero if $a_i = a_j$. Consequently, if two pixels have similar predictions, only a small gradient is propagated through the feature similarity loss, and the total gradient is dominated by the classification loss. This allows the network to classify larger regions to the same class, even though they contain parts with dissimilar features. Thus, the network can activate over the whole extent of objects.

We use RGB pixel values in $[0, 1]$ for the features x , and choose the dissimilarity

$$d(x_i, x_j) = \frac{\|x_i - x_j\|_1}{C}, \quad (13)$$

which has been used in stereo matching [33], where $C = 3$ is the dimensionality of the feature vectors. Although learnable features would allow for finding image-specific biases, they could potentially lead to trivial solutions or unwanted behaviours if combined with the classification loss, as we would essentially be learning the loss function. Therefore, we stick to RGB features.

4 EXPERIMENTS

This section outlines the experimental results achieved for the methods described above. Section 4.1 details the implementation of training and inference as well as the data used. In Sec. 4.2 we perform ablation studies to demonstrate the effect of our contributions. Subsequently, in Sec. 4.3 we compare our results to our baseline method, SEAM [4]. Finally, in Sec. 4.4 we compare our results to current state-of-the-art methods within WSSS.

4.1 Implementation Details

Dataset. For training and evaluation we use the *PASCAL Visual Object Classes* (VOC) dataset [34] containing 1,464 training images, 1,449 validation images and 1,456 hold-out test images, with 20 foreground classes. Furthermore, we include the training data proposed by Hariharan et al. [35], which is common in VOC experiments, resulting in a total of 10,582 training images. Although ground-truth segmentation masks are available, we only use image-level classification labels for training.

Evaluation metrics. For evaluation, we use the commonly adopted mean intersection-over-union (mIoU) metric, or Jaccard index [36], based on the area of the segmentations to measure region similarity, denoted \mathcal{J} . Additionally, we suggest to further evaluate WSSS methods by measuring contour quality using the F-score computed on the segmentation mask contours, denoted \mathcal{F} . We also measure a combined score which is simply an average of the two metrics, denoted $\mathcal{J\&F}$. The use of the contour F-score metric is motivated by the fact that it captures a complementary aspect compared to region similarity. Depending on the downstream task, one aspect might be more important than the other. For example, contours contribute more to the perceived visual quality [11], and bear more weight in cases where the segmentations are displayed to a human, such as in virtual green-screen applications. Since we do not consider a specific application, it is important to evaluate both aspects simultaneously. The same reasoning has been utilized in similar computer vision tasks, such as in the well-established DAVIS video object segmentation benchmark, which measures both region similarity and contour quality, as well as the combined metric $\mathcal{J\&F}$ [12]. To the best of our knowledge, we are the first to apply this to WSSS.

We adapt the code from Perazzi et al. [12] and compute the F-score by first accumulating bipartite matches of the boundaries between the predicted and ground-truth masks, efficiently approximated using morphological operations.

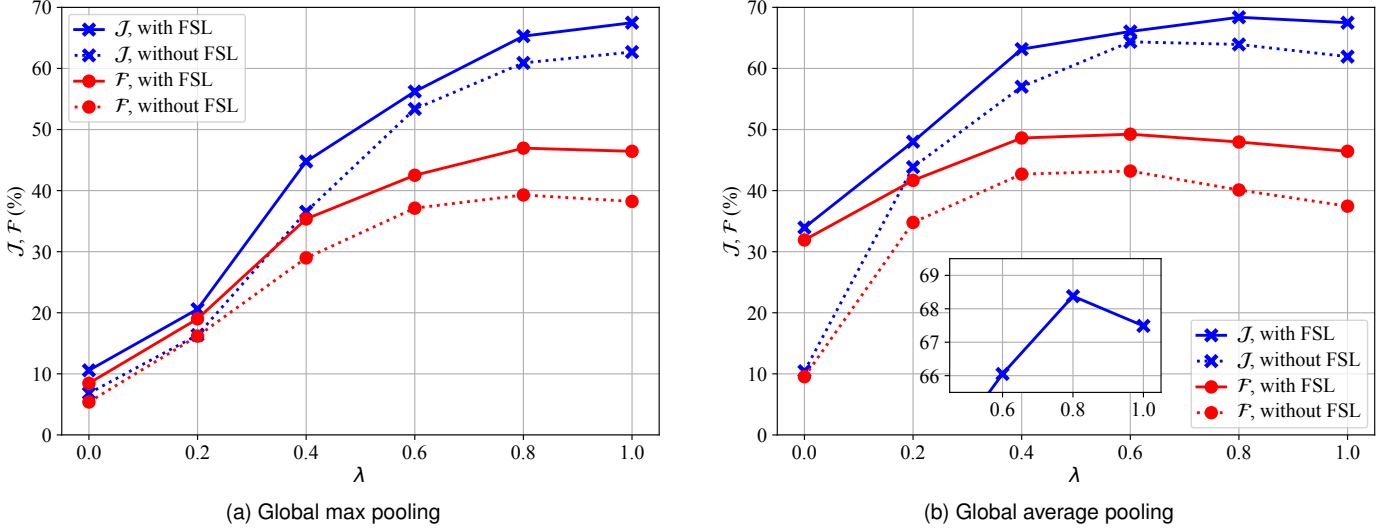


Fig. 3. Region similarity (\mathcal{J}) and contour quality (\mathcal{F}) on the VOC training set for final segmentations, as functions of the loss parameter λ , with and without the feature similarity loss (FSL), for (a) global max pooling, and (b) global average pooling. FSL parameters are set to $\mu = 2$ and $\sigma = 5$.

Subsequently, we compute the class-wise F-scores over the dataset, which we then average. Although the VOC segmentation masks contain a thin no-class region between objects, the contour F-score still gives a clear indication of the contour quality since we match the boundaries using dilated regions. Thus, we compute the contour quality by considering this thin no-class region as background.

Training details. For our CAM network we use the same siamese architecture as our baseline method SEAM [4] with a ResNet-38 [37] backbone. As part of the architecture, we also incorporate their method of refining the CAMs using a pixel correlation module (PCM) in the final layer of the network, and adopt their equivariant regularization (ER) and equivariant cross regularization (ECR) loss terms. Thus, our loss function has four terms, namely \mathcal{L}_{cls} , \mathcal{L}_{fs} , \mathcal{L}_{er} and \mathcal{L}_{ecr} . We simply sum the four terms, which corresponds to a weight of 1 for each of them, similar to SEAM (for \mathcal{L}_{cls} , \mathcal{L}_{er} , and \mathcal{L}_{ecr}). We perform minor adjustments to the forward method of the network and the inference scheme to fit with our probabilistic formulation according to (1), (5) and (6). In order to measure the effects of our contributions we do not change any settings or hyperparameters, such as input image dimensions, data augmentation, batch size, number of epochs, optimizer, learning rate, or learning rate schedule. We randomly rescale the input image such that the longest edge is in $[448, 768]$ and extract a crop of size 448×448 for the network input. A list of hyperparameters and other settings can be found in Table 1. For a fair comparison, we follow the framework in SEAM of training an AffinityNet [6] to further refine the CAMs before pseudo-label generation. During AffinityNet label generation, we modify the background parameter α to 2 and 4 when amplifying and weakening the background activations respectively. This was necessary as the values in our CAMs were distributed close to either 0 or 1, while the CAMs from SEAM were distributed more evenly over $[0, 1]$. Other than that, we use the same settings and hyperparameters for AffinityNet training. During pseudo-label generation,

TABLE 1
Hyperparameters and settings

Name	Value
Backbone	ResNet-38
Random image rescale interval	$[448, 768]$
Random crop size (network input)	448
Output stride	8
Batch size	8
Epochs	8
Optimizer	SGD
Initial learning rate, α_{init}	0.01
Learning rate policy (at iteration i)	$\alpha_{init} \left(1 - \frac{i}{i_{max}}\right)^\gamma$
Decay parameter, γ	0.9
Momentum	0.9
Weight decay	$5 \cdot 10^{-4}$

we remove segmentation masks for classes that are not present in the image. This information is available in the image-level classification label. As the last step, we train a DeepLab-v1 [38] network as our final segmentation model, which is supervised by our generated pseudo-labels from the CAM and AffinityNet networks. Both the AffinityNet and DeepLab-v1 networks have the same ResNet-38 [37] backbone as our CAM network. Similar to SEAM, we use CRF [27] to produce our segmentation predictions during inference. In our experiments we use two A100 40GB GPUs.

4.2 Ablation Study

To investigate the effects of the *importance sampling* and *feature similarity loss* (FSL) we train our model on the VOC dataset and compare region similarity in terms of mIoU based on the area of predicted segmentations, as well as contour quality in terms of the F-score computed on the contours. All ablations are evaluated on the training set since we use the validation data as a test set to compare with previous methods in subsequent sections. Note, however, that the tuning of hyperparameters differs from the fully

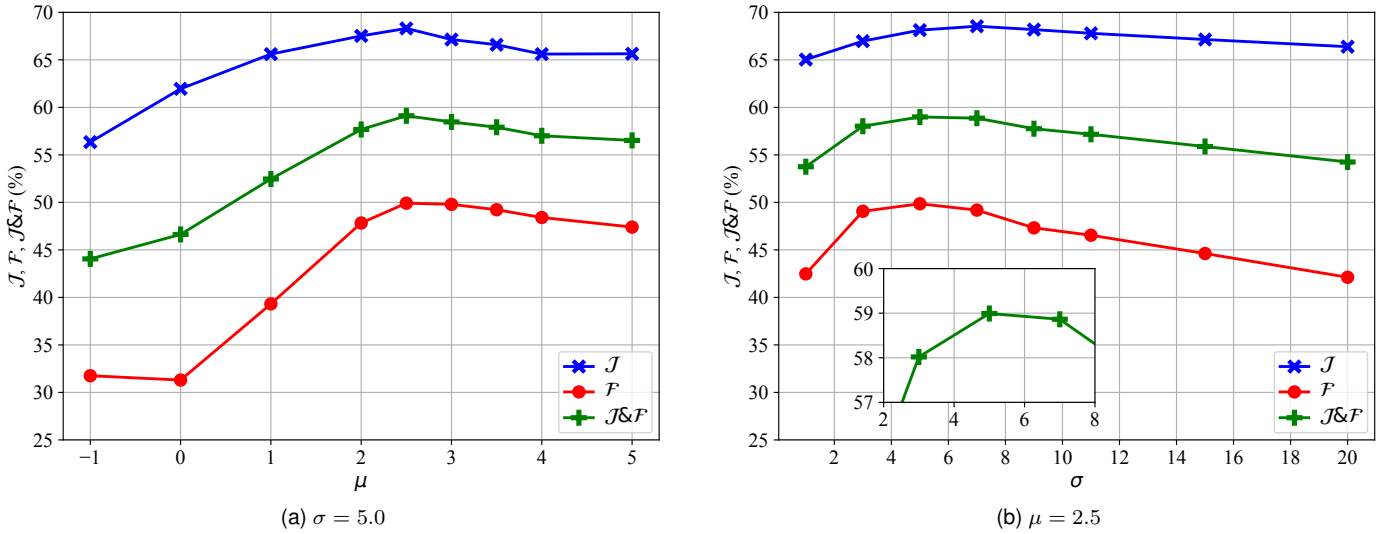


Fig. 4. Region similarity (\mathcal{J}), contour quality (\mathcal{F}), and averaged ($\mathcal{J}\&\mathcal{F}$) on the VOC training set for final segmentations, as functions of (a) μ , and (b) σ .

supervised setting since the model training does not involve full segmentation labels, while the evaluation does. Thus, different data is used for training and evaluation, reducing the risk of overfitting. Nevertheless, we observed similar results on the validation and training sets.

4.2.1 Importance Sampling Loss Weight

In Fig. 3 we sweep the loss parameter λ from (8) for global max pooling (GMP) and global average pooling (GAP), and plot the region similarity and contour quality for final segmentations. With max pooling in Fig. 3a we observe a significant increase in segmentation performance when increasing λ , both in terms of region similarity and contour quality. The highest performance in terms of region similarity occurs at $\lambda = 1$, and for contour quality at 0.8. This is due to the fact that the classification loss is computed based on more than just the most activated pixel and thus encourages the model to activate over more than just the most discriminant feature. If the model activates over *any* class-specific feature, those pixels will be sampled during training and thus the model can learn to associate these features with the corresponding class. We can observe this in Fig. 2. With GMP only, the model activates over the most discriminant features, e.g. faces of persons. With importance sampling, it has learned to activate also over other features, such as hands and legs. Similarly, if the model activates over features that are not associated with a certain class it will get penalized in cases where those features are present but not the class. Thus, it will learn to activate only over the objects themselves.

With GAP in Fig. 3b we see a similar trend of better region similarity for larger values of λ . However, the maximum region similarity occurs at $\lambda = 0.8$ which indicates that a combination of GAP and importance sampling is better than using only one or the other. We hypothesize that average pooling contributes with a regularizing effect by effectively introducing a bias to the probability distributions p_k in (5). As explained in Sec. 3.2, GAP corresponds to a

uniform distribution. The combination of GAP and importance sampling would then correspond to using a mixture of the activation-based and uniform distributions, and the resulting distribution would be similar to the activation-based distribution but with a non-zero minimum, i.e. a bias. The specific value of $\lambda = 0.8$ indicates that this bias should be quite small. The maximum for the contour F-score occurs at a different value of λ , at 0.6. However, the combined metric $\mathcal{J}\&\mathcal{F}$ for $\lambda = 0.8$ is slightly higher at 58.2, compared to 57.6 for $\lambda = 0.6$, so we choose $\lambda = 0.8$ with GAP for the rest of our experiments.

4.2.2 Effect of the Feature Similarity Loss

In Figure 3 we see that the feature similarity loss term gives a performance boost across the board. Both region similarity and contour quality is improved for all values of λ . This is the case for both GMP and GAP. Next, we search for optimal values for the FSL-specific parameters, namely the standard deviation σ , and the bias parameter μ . First, we fix $\sigma = 5.0$ and plot region similarity and contour quality as functions of μ in Figure 4a. The maximum occurs at 2.5 for both metrics. Subsequently, we fix $\mu = 2.5$ and plot \mathcal{J} , \mathcal{F} , and $\mathcal{J}\&\mathcal{F}$ as functions of σ in Figure 4b. The optimal standard deviation occurs at 7 for the region similarity, and at 5 for the contour quality. However, the region similarity only changes slightly between these values, while the change in contour quality is more notable. This means that the highest combined score is at $\sigma = 5$. Thus, we choose $\sigma = 5$ for the rest of our experiments, as it provides a good balance between the two metrics.

The bias parameter μ in (12) controls what should be considered similar or dissimilar when looking at the difference in RGB values of pixel pairs. A value of 0 means that the breaking point between similar and dissimilar occurs when the normalized L1 distance d between RGB values is 0.5, i.e. the point at which the sign of \mathcal{L}_{fs} flips. A positive bias pushes the breaking point lower, meaning that pixels need to be more similar in color in order to be considered

TABLE 2

Region similarity (\mathcal{J}), contour quality (\mathcal{F}), and averaged ($\mathcal{J}\&\mathcal{F}$) on the VOC training set when varying the number of sampled pixels. Mean and standard deviation is reported over five runs

#pixels	\mathcal{J}	\mathcal{F}	$\mathcal{J}\&\mathcal{F}$
1	65.9 \pm 3.6	48.5 \pm 2.3	57.2 \pm 3.0
2	67.6 \pm 1.3	49.1 \pm 1.3	58.3 \pm 1.3
5	68.0 \pm 0.5	49.8 \pm 0.5	58.9 \pm 0.5
10	68.3 \pm 0.2	49.5 \pm 0.4	58.9 \pm 0.3
20	68.3 \pm 0.5	49.6 \pm 0.4	58.9 \pm 0.5
50	68.2 \pm 0.4	49.6 \pm 0.4	58.9 \pm 0.4
100	68.4 \pm 0.3	49.8 \pm 0.2	59.1 \pm 0.2

similar. An optimum at $\mu = 2.5$ implies that $d < 0.076$ is required for two pixels to be considered similar.

To conclude, we fix $\mu = 2.5$, and $\sigma = 5$ for the rest of our experiments.

4.2.3 Number of Sampled Pixels

Hypothetically, sampling several pixels during importance sampling enables more efficient learning and better CAMs. Therefore, we evaluate our method under a varying number of sampled pixels and average the classification loss \mathcal{L}_{cls} accordingly. Tab. 2 shows the mean and standard deviation of \mathcal{J} , \mathcal{F} , and $\mathcal{J}\&\mathcal{F}$ over five runs on final segmentation predictions. We observe that the performance increases with a larger number of sampled pixels, while the standard deviation decreases at the same time. Furthermore, we observed that, while the maximum score over five runs was only affected slightly, the training could diverge in the early parts of training when using a small number of sampled pixels, resulting in low scores. We did not observe this behaviour for a larger number of pixels. This could be the result of a few unlucky samples during the early iterations, causing the training to become unstable since the predictions are mostly random at this stage. Using more pixels leads to a less sporadic behaviour, and thus, avoids divergence in the early parts of training. Thus, we set the number of samples to 100 for the subsequent experiments.

4.2.4 Qualitative Results

For a qualitative assessment, we display in Fig. 5 the foreground class activations, together with CAM pseudo-labels and final predictions. Our method manages to successfully segment the images with impressive contour quality, even in low contrast conditions, e.g. black suit on dark background on the fourth row. However, it is less successful on thin structures, e.g. boat masts, or table and chair legs on rows five and six respectively.

4.3 Baseline Comparison

We train our segmentation model in the three stages described previously and evaluate the segmentation performance after each stage in terms of (1) CAM pseudo-labels, (2) AffinityNet pseudo-labels, and (3) final segmentation masks. We do the same for our baseline SEAM [4] and compare the results in Tab. 3, where we measure both region similarity and contour contour quality. Note that the first two rows comparing CAM and AffinityNet results show

TABLE 3

Baseline comparison with SEAM [4] in terms of region similarity (\mathcal{J}), contour quality (\mathcal{F}), and averaged ($\mathcal{J}\&\mathcal{F}$), on the VOC validation set, for CAM and AffinityNet pseudo-labels, and final segmentations. Mean is reported over five runs

Pseudo-labels/ segmentations	\mathcal{J}		\mathcal{F}		$\mathcal{J}\&\mathcal{F}$	
	SEAM	Ours	SEAM	Ours	SEAM	Ours
CAMs	52.5	57.2	20.8	40.8	36.7	49.0
AffinityNet	60.1	65.2	35.7	48.9	47.9	57.0
Final	64.6	67.2	39.4	47.9	52.0	57.6

TABLE 4

Region similarity (\mathcal{J}), contour quality (\mathcal{F}), and combined ($\mathcal{J}\&\mathcal{F}$) on the VOC validation set, comparing our contributions separately on SEAM. Mean is reported over five runs

Method	\mathcal{J}	\mathcal{F}	$\mathcal{J}\&\mathcal{F}$
SEAM	64.6	39.4	52.0
SEAM + importance sampling	62.5	41.6	52.1
SEAM + feature similarity loss	65.2	43.6	54.4
Ours	67.2	47.9	57.6

the metrics computed for pseudo-labels without CRF. The last row compares the results of the final segmentation predictions where CRF has been applied. We observe that our method has significantly better contour quality across the board. The difference is most notable for the CAM results, where we reach an F-score of 40.8 compared to 20.8 for SEAM. Furthermore, the property of accurate contours carries through to the final segmentation model. Both methods benefit from training an AffinityNet where the contour quality and region similarity increase for both methods. We also observe an improvement in terms of region similarity where we reach 67.2 mIoU compared to 64.6 for SEAM.

Table 4 compares the results from SEAM [4] with our contributions implemented separately. Importance sampling alone slightly reduces the region similarity by -2.1 points, but makes up for it in contour quality, increasing it by +2.2 points. The feature similarity loss, on the other hand, yields strong improvements in both metrics, and results in an increase in the combined score of +2.4 points. Applying both our contributions at once, i.e. yielding our method, results in even stronger improvements, especially in contour quality, which increases by +8.5 points compared to the baseline. In terms of the combined score, our contributions yield strict improvements over the baseline, and when combined, results in an improvement of +5.6 points.

4.4 State-of-the-art Comparison

To push the limits of our method even further, we employ a Pretended Under-Fitting strategy and Cyclic Pseudo-masks from PMM [39] during the final training stage. Furthermore, we substitute the ResNet-38 architecture in the final stage for the more powerful Res2Net-101 [40] backbone, which has shown to be effective in WSSS [39]. We refer to this setting as extended training (et).

In Tab. 5, we evaluate some state-of-the-art methods in terms of both region similarity and contour quality. This

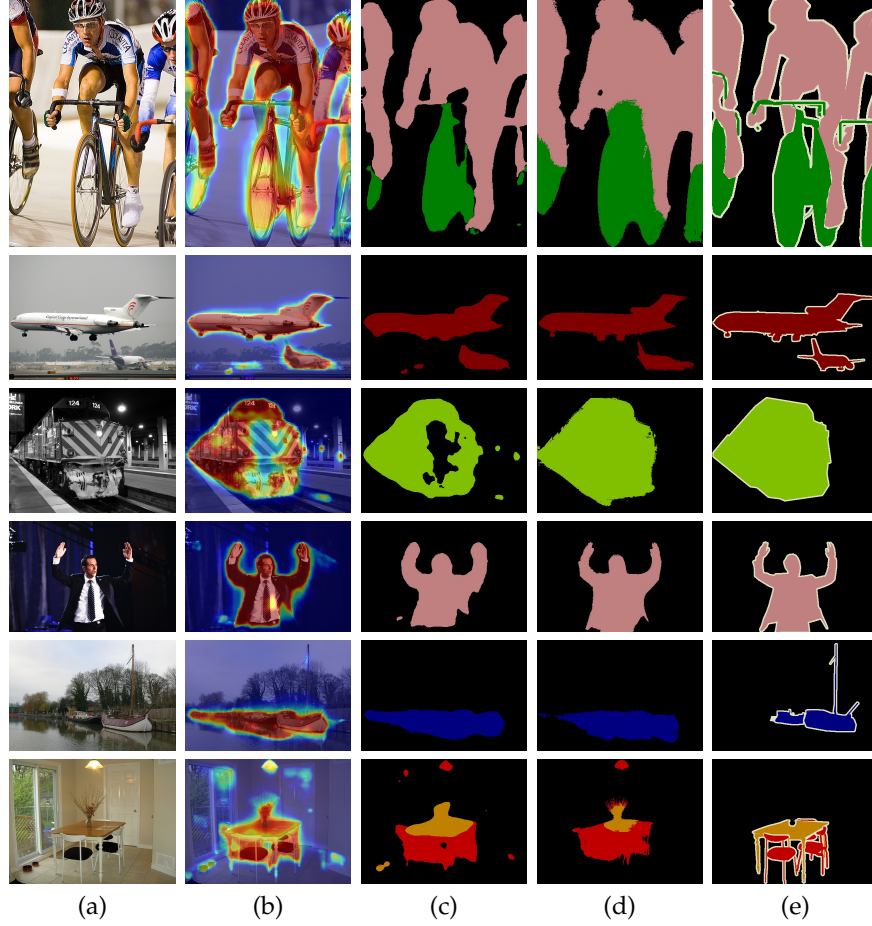


Fig. 5. Qualitative segmentation results. (a) Input image, (b) foreground class activations, (c) pseudo-labels from our CAM network, (d) final segmentation predictions and (e) ground-truth segmentations. The bottom two rows illustrate failure cases.

TABLE 5

Region similarity (\mathcal{J}), contour quality (\mathcal{F}), and averaged ($\mathcal{J}\&\mathcal{F}$) on the VOC validation set. All values are reproduced from the original implementations, and averaged over five runs. *fp* is short for fixed parameters, and *et* indicates extended training from PMM

Method	Backb.	\mathcal{J}	\mathcal{F}	$\mathcal{J}\&\mathcal{F}$
SEAM [4]	Res38	64.6 ± 0.1	39.4 ± 1.5	52.0 ± 0.7
CDA [41]	Res38	63.7 ± 0.1	42.7 ± 0.1	53.2 ± 0.1
PMM [39]	Res38	67.3 ± 0.2	46.4 ± 0.3	56.9 ± 0.2
PMM [39]	R2N	68.8 ± 0.7	48.9 ± 0.5	58.8 ± 0.6
MCTformer [42]	DeiT-S	<u>71.0 ± 0.2</u>	47.6 ± 0.3	59.3 ± 0.2
<hr/>				
	<i>fp et</i>			
ICAM [13]	Res38	63.9 ± 0.6	43.5 ± 0.8	53.7 ± 0.7
ICAM (ours) ✓	Res38	67.2 ± 0.3	47.9 ± 0.3	57.6 ± 0.2
ICAM (ours) ✓ ✓	Res38	69.1 ± 0.5	48.2 ± 0.6	58.6 ± 0.5
ICAM (ours) ✓ ✓	R2N	70.1 ± 0.2	<u>50.3 ± 0.4</u>	<u>60.2 ± 0.3</u>

was only possible for methods where a code implementation was readily available, since reproducing the final segmentations was necessary for computing the contour F-score. The table shows the metrics after re-running the codes, including re-training unless weights or pseudo-labels were provided, in order to reproduce the original results as closely as possible. Note, however, that this leads to a lower expected variance for the previous methods where these were available, since the training was resumed from

TABLE 6

Region similarity comparison on the VOC validation and test sets. All values are taken from their respective publications

Method	<i>val</i>	<i>test</i>	Method	<i>val</i>	<i>test</i>
CCNN [20]	35.3	35.6	MCIS [49]	66.2	66.9
EM-Adapt [16]	38.2	39.6	PPC [50]	67.7	67.4
SEC [21]	50.7	51.7	ECS-Net [51]	66.6	67.6
AugFeed [43]	54.3	55.5	CGNet [52]	68.4	68.2
AffinityNet [6]	61.7	63.7	ReCAM [53]	68.5	68.4
ICD [44]	64.1	64.3	CPN [54]	67.8	68.5
CIAN [45]	64.3	65.3	RIB [55]	68.3	68.6
SSDD [46]	64.9	65.5	SIPE [56]	68.8	69.7
SEAM [4]	64.5	65.7	PMM [39]	70.0	70.5
AFA [47]	66.0	66.3	MCTformer [42]	71.9	71.6
CONTA [48]	66.1	66.7	SANCE [57]	70.9	72.2
CDA [41]	66.1	66.8	ICAM (ours)	70.1	70.8

a later stage, as opposed to started from scratch. Thus, the variance in the preceding stages is eliminated. In the table, we denote our method ICAM, short for *Importance Sampling CAMs*. In the comparison, we include our early version [13] of ICAM which sets μ and σ to learnable parameters, uses one sampled pixel per class during importance sampling, and sets $\lambda = 1$. This setting is distinguished by the fixed parameters (*fp*) column in the bottom half of Tab. 5. In this paper, we fix the parameters μ and σ according to Fig. 4,

which is indicated by the check mark in this column. Our final method reaches a high region similarity score of 70.1, which is not far off the best previous method. Moreover, we reach the highest contour quality of 50.3, which is +1.4 points better than PMM [39] which is the second best in this metric. Finally, for the combined metric $\mathcal{J}\&\mathcal{F}$, we achieve a score of 60.2, which is the highest score in this comparison, beating the best previous method, MCTformer [42], by +0.9 points. To conclude, the results show that our method is well balanced in these two complementary aspects, and an all-around method suitable for a wide range of applications.

In Tab. 6 we compare the region similarity on the VOC validation and test sets, with previous WSSS methods as reported in the respective papers. We have excluded methods which make use of additional supervision, either directly using other datasets, or indirectly using saliency maps. For ICAM, we show the result using the extended training and a Res2Net-101 backbone, corresponding to the last row in Tab. 5. We submit the test set segmentation predictions of our best model to the official PASCAL VOC evaluation server to attain the score on the test set. Similar to Tab. 5, we reach a region similarity score close to the current state-of-the-art in weakly-supervised semantic segmentation, which shows that we can improve the contour quality without sacrificing region similarity performance.

5 CONCLUSIONS

We present two methods for improving CAM learning in weakly-supervised semantic segmentation (WSSS). First, we use importance sampling for producing stochastic image-level predictions during training, which results in CAMs that cover a larger extent of the objects. Second, we propose a new feature similarity loss term for aligning prediction contours with edges in the image. Furthermore, we find that previous methods somewhat lack in contour quality and suggest to explicitly evaluate WSSS methods in terms of contour F-score, similar to related computer vision tasks. We find experimentally, that our method outperforms previous methods in terms of contour quality, while being comparable to state-of-the-art methods in terms of region similarity. Considering the two metrics equally, our method outright outperforms the previous state-of-the-art methods. Thus, it is more suitable for a wider range of applications.

ACKNOWLEDGMENTS

This work was partially supported by the Wallenberg AI, Autonomous Systems and Software Program (WASP) funded by the Knut and Alice Wallenberg (KAW) Foundation. The computations were conducted at the Berzelius SuperPOD, provided by the National Supercomputer Centre (NSC), and at the Alvis cluster, provided by the Swedish National Infrastructure for Computing (SNIC), partially funded by the Swedish Research Council (VR) through grant agreement no. 2018-05973.

REFERENCES

- [1] M. Cordts, M. Omran, S. Ramos, T. Rehfeld, M. Enzweiler, R. Benenson, U. Franke, S. Roth, and B. Schiele, "The cityscapes dataset for semantic urban scene understanding," in *Proceedings of the IEEE Conference on Computer Vision and Pattern Recognition (CVPR)*, 2016.
- [2] M. Gruosso, N. Capece, and U. Erra, "Human segmentation in surveillance video with deep learning," *Multimedia Tools and Applications*, vol. 80, no. 1, pp. 1175–1199, 2021.
- [3] S. Minaee, Y. Y. Boykov, F. Porikli, A. J. Plaza, N. Kehtarnavaz, and D. Terzopoulos, "Image segmentation using deep learning: A survey," *IEEE Transactions on Pattern Analysis and Machine Intelligence*, 2021.
- [4] Y. Wang, J. Zhang, M. Kan, S. Shan, and X. Chen, "Self-supervised equivariant attention mechanism for weakly supervised semantic segmentation," in *Proceedings of the IEEE/CVF Conference on Computer Vision and Pattern Recognition*, 2020, pp. 12 275–12 284.
- [5] B. Zhou, A. Khosla, A. Lapedriza, A. Oliva, and A. Torralba, "Learning deep features for discriminative localization," in *Proceedings of the IEEE Conference on Computer Vision and Pattern Recognition*, 2016, pp. 2921–2929.
- [6] J. Ahn and S. Kwak, "Learning pixel-level semantic affinity with image-level supervision for weakly supervised semantic segmentation," in *Proceedings of the IEEE Conference on Computer Vision and Pattern Recognition*, 2018, pp. 4981–4990.
- [7] J. Lee, E. Kim, S. Lee, J. Lee, and S. Yoon, "Ficklenet: Weakly and semi-supervised semantic image segmentation using stochastic inference," in *Proceedings of the IEEE/CVF Conference on Computer Vision and Pattern Recognition*, 2019, pp. 5267–5276.
- [8] N. J. Gordon, D. J. Salmond, and A. F. Smith, "Novel approach to nonlinear/non-gaussian bayesian state estimation," in *IEEE Proceedings on Radar and Signal Processing*, vol. 140. IET, 1993, pp. 107–113.
- [9] M. A. Fischler and R. C. Bolles, "Random sample consensus: A paradigm for model fitting with applications to image analysis and automated cartography," *Communications of the ACM*, vol. 24, no. 6, pp. 381–395, 1981.
- [10] D. Robinson, "The mechanics of human saccadic eye movement," *The Journal of Physiology*, vol. 174, no. 2, p. 245, 1964.
- [11] G. Csúrká, D. Larlus, and F. Perronnin, "What is a good evaluation measure for semantic segmentation?" in *Proceedings of the British Machine Vision Conference (BMVC)*, vol. 27, 2013.
- [12] F. Perazzi, J. Pont-Tuset, B. McWilliams, L. Van Gool, M. Gross, and A. Sorkine-Hornung, "A benchmark dataset and evaluation methodology for video object segmentation," in *Proceedings of the IEEE Conference on Computer Vision and Pattern Recognition*, 2016, pp. 724–732.
- [13] A. Jonnarth and M. Felsberg, "Importance sampling CAMs for weakly-supervised segmentation," in *IEEE International Conference on Acoustics, Speech, and Signal Processing (ICASSP)*, 2022, pp. 2639–2643.
- [14] J. Dai, K. He, and J. Sun, "Boxsup: Exploiting bounding boxes to supervise convolutional networks for semantic segmentation," in *Proceedings of the IEEE International Conference on Computer Vision*, 2015, pp. 1635–1643.
- [15] A. Khoreva, R. Benenson, J. Hosang, M. Hein, and B. Schiele, "Simple does it: Weakly supervised instance and semantic segmentation," in *Proceedings of the IEEE Conference on Computer Vision and Pattern Recognition*, 2017, pp. 876–885.
- [16] G. Papandreou, L.-C. Chen, K. P. Murphy, and A. L. Yuille, "Weakly- and semi-supervised learning of a deep convolutional network for semantic image segmentation," in *Proceedings of the IEEE International Conference on Computer Vision*, 2015, pp. 1742–1750.
- [17] D. Lin, J. Dai, J. Jia, K. He, and J. Sun, "Scribblesup: Scribble-supervised convolutional networks for semantic segmentation," in *Proceedings of the IEEE Conference on Computer Vision and Pattern Recognition*, 2016, pp. 3159–3167.
- [18] P. Vernaza and M. Chandraker, "Learning random-walk label propagation for weakly-supervised semantic segmentation," in *Proceedings of the IEEE Conference on Computer Vision and Pattern Recognition*, 2017, pp. 7158–7166.
- [19] A. Bearman, O. Russakovsky, V. Ferrari, and L. Fei-Fei, "What's the point: Semantic segmentation with point supervision," in *European Conference on Computer Vision*. Springer, 2016, pp. 549–565.
- [20] D. Pathak, P. Krähenbühl, and T. Darrell, "Constrained convolutional neural networks for weakly supervised segmentation," in *Proceedings of the IEEE International Conference on Computer Vision*, 2015, pp. 1796–1804.
- [21] A. Kolesnikov and C. H. Lampert, "Seed, expand and constrain: Three principles for weakly-supervised image segmentation," in *European Conference on Computer Vision*. Springer, 2016, pp. 695–711.

- [22] Y. Wei, X. Liang, Y. Chen, X. Shen, M.-M. Cheng, J. Feng, Y. Zhao, and S. Yan, "Stc: A simple to complex framework for weakly-supervised semantic segmentation," *IEEE Transactions on Pattern Analysis and Machine Intelligence*, vol. 39, no. 11, pp. 2314–2320, 2016.
- [23] R. R. Selvaraju, M. Cogswell, A. Das, R. Vedantam, D. Parikh, and D. Batra, "Grad-cam: Visual explanations from deep networks via gradient-based localization," in *Proceedings of the IEEE International Conference on Computer Vision*, 2017, pp. 618–626.
- [24] M. Oquab, L. Bottou, I. Laptev, and J. Sivic, "Is object localization for free? - weakly-supervised learning with convolutional neural networks," in *Proceedings of the IEEE Conference on Computer Vision and Pattern Recognition*, 2015, pp. 685–694.
- [25] T. Durand, T. Mordan, N. Thome, and M. Cord, "WILDCAT: Weakly supervised learning of deep convnets for image classification, pointwise localization and segmentation," in *Proceedings of the IEEE Conference on Computer Vision and Pattern Recognition*, 2017, pp. 642–651.
- [26] A. Buades, B. Coll, and J.-M. Morel, "Non-local means denoising," *Image Processing On Line*, vol. 1, pp. 208–212, 2011.
- [27] P. Krähenbühl and V. Koltun, "Efficient inference in fully connected crfs with gaussian edge potentials," *Advances in Neural Information Processing Systems*, vol. 24, pp. 109–117, 2011.
- [28] Y. Liu, Y.-H. Wu, P.-S. Wen, Y.-J. Shi, Y. Qiu, and M.-M. Cheng, "Leveraging instance-, image- and dataset-level information for weakly supervised instance segmentation," *IEEE Transactions on Pattern Analysis and Machine Intelligence*, 2020.
- [29] C. Bucilua, R. Caruana, and A. Niculescu-Mizil, "Model compression," in *Proceedings of the 12th ACM SIGKDD International Conference on Knowledge Discovery and Data Mining*, 2006, pp. 535–541.
- [30] G. Hinton, O. Vinyals, and J. Dean, "Distilling the knowledge in a neural network," *arXiv preprint arXiv:1503.02531*, 2015.
- [31] Z. Allen-Zhu and Y. Li, "Towards understanding ensemble, knowledge distillation and self-distillation in deep learning," *arXiv preprint arXiv:2012.09816*, 2020.
- [32] C. Tomasi and R. Manduchi, "Bilateral filtering for gray and color images," in *Sixth International Conference on Computer Vision*. IEEE, 1998, pp. 839–846.
- [33] M. Galar, A. Jurio, C. Lopez-Molina, D. Paternain, J. Sanz, and H. Bustince, "Aggregation functions to combine rgb color channels in stereo matching," *Optics express*, vol. 21, no. 1, pp. 1247–1257, 2013.
- [34] M. Everingham, L. Van Gool, C. K. Williams, J. Winn, and A. Zisserman, "The pascal visual object classes (voc) challenge," *International Journal of Computer Vision*, vol. 88, no. 2, pp. 303–338, 2010.
- [35] B. Hariharan, P. Arbeláez, L. Bourdev, S. Maji, and J. Malik, "Semantic contours from inverse detectors," in *2011 International Conference on Computer Vision*. IEEE, 2011, pp. 991–998.
- [36] P. Jaccard, "Distribution de la flore alpine dans le bassin des dranses et dans quelques régions voisines," *Bulletin de la Société Vaudoise des Sciences Naturelles*, vol. 37, pp. 241–272, 1901.
- [37] Z. Wu, C. Shen, and A. Van Den Hengel, "Wider or deeper: Revisiting the resnet model for visual recognition," *Pattern Recognition*, vol. 90, pp. 119–133, 2019.
- [38] L.-C. Chen, G. Papandreou, I. Kokkinos, K. Murphy, and A. L. Yuille, "Semantic image segmentation with deep convolutional nets and fully connected crfs," in *International Conference on Learning Representations*, 2015.
- [39] Y. Li, Z. Kuang, L. Liu, Y. Chen, and W. Zhang, "Pseudo-mask matters in weakly-supervised semantic segmentation," in *Proceedings of the IEEE/CVF International Conference on Computer Vision (ICCV)*, October 2021, pp. 6964–6973.
- [40] S.-H. Gao, M.-M. Cheng, K. Zhao, X.-Y. Zhang, M.-H. Yang, and P. Torr, "Res2net: A new multi-scale backbone architecture," *IEEE Transactions on Pattern Analysis and Machine Intelligence*, vol. 43, no. 2, pp. 652–662, 2021.
- [41] Y. Su, R. Sun, G. Lin, and Q. Wu, "Context decoupling augmentation for weakly supervised semantic segmentation," in *Proceedings of the IEEE/CVF International Conference on Computer Vision (ICCV)*, October 2021, pp. 7004–7014.
- [42] L. Xu, W. Ouyang, M. Bennamoun, F. Boussaid, and D. Xu, "Multi-class token transformer for weakly supervised semantic segmentation," in *Proceedings of the IEEE/CVF Conference on Computer Vision and Pattern Recognition (CVPR)*, June 2022, pp. 4310–4319.
- [43] X. Qi, Z. Liu, J. Shi, H. Zhao, and J. Jia, "Augmented feedback in semantic segmentation under image level supervision," in *European Conference on Computer Vision*. Springer, 2016, pp. 90–105.
- [44] J. Fan, Z. Zhang, C. Song, and T. Tan, "Learning integral objects with intra-class discriminator for weakly-supervised semantic segmentation," in *Proceedings of the IEEE/CVF Conference on Computer Vision and Pattern Recognition*, 2020, pp. 4283–4292.
- [45] J. Fan, Z. Zhang, T. Tan, C. Song, and J. Xiao, "Cian: Cross-image affinity net for weakly supervised semantic segmentation," in *Proceedings of the AAAI Conference on Artificial Intelligence*, vol. 34, 2020, pp. 10762–10769.
- [46] W. Shimoda and K. Yanai, "Self-supervised difference detection for weakly-supervised semantic segmentation," in *Proceedings of the IEEE/CVF International Conference on Computer Vision*, 2019, pp. 5208–5217.
- [47] L. Ru, Y. Zhan, B. Yu, and B. Du, "Learning affinity from attention: End-to-end weakly-supervised semantic segmentation with transformers," in *Proceedings of the IEEE/CVF Conference on Computer Vision and Pattern Recognition (CVPR)*, June 2022, pp. 16846–16855.
- [48] D. Zhang, H. Zhang, J. Tang, X.-S. Hua, and Q. Sun, "Causal intervention for weakly-supervised semantic segmentation," in *Advances in Neural Information Processing Systems*, H. Larochelle, M. Ranzato, R. Hadsell, M. F. Balcan, and H. Lin, Eds., vol. 33. Curran Associates, Inc., 2020, pp. 655–666.
- [49] G. Sun, W. Wang, J. Dai, and L. Van Gool, "Mining cross-image semantics for weakly supervised semantic segmentation," in *European conference on computer vision*. Springer, 2020, pp. 347–365.
- [50] Y. Du, Z. Fu, Q. Liu, and Y. Wang, "Weakly supervised semantic segmentation by pixel-to-prototype contrast," in *Proceedings of the IEEE/CVF Conference on Computer Vision and Pattern Recognition (CVPR)*, June 2022, pp. 4320–4329.
- [51] K. Sun, H. Shi, Z. Zhang, and Y. Huang, "Ecs-net: Improving weakly supervised semantic segmentation by using connections between class activation maps," in *Proceedings of the IEEE/CVF International Conference on Computer Vision (ICCV)*, October 2021, pp. 7283–7292.
- [52] H. Kweon, S.-H. Yoon, H. Kim, D. Park, and K.-J. Yoon, "Unlocking the potential of ordinary classifier: Class-specific adversarial erasing framework for weakly supervised semantic segmentation," in *Proceedings of the IEEE/CVF International Conference on Computer Vision (ICCV)*, October 2021, pp. 6994–7003.
- [53] Z. Chen, T. Wang, X. Wu, X.-S. Hua, H. Zhang, and Q. Sun, "Class re-activation maps for weakly-supervised semantic segmentation," in *Proceedings of the IEEE/CVF Conference on Computer Vision and Pattern Recognition (CVPR)*, June 2022, pp. 969–978.
- [54] F. Zhang, C. Gu, C. Zhang, and Y. Dai, "Complementary patch for weakly supervised semantic segmentation," in *Proceedings of the IEEE/CVF International Conference on Computer Vision*, 2021, pp. 7242–7251.
- [55] J. Lee, J. Choi, J. Mok, and S. Yoon, "Reducing information bottleneck for weakly supervised semantic segmentation," *Advances in Neural Information Processing Systems*, vol. 34, 2021.
- [56] Q. Chen, L. Yang, J.-H. Lai, and X. Xie, "Self-supervised image-specific prototype exploration for weakly supervised semantic segmentation," in *Proceedings of the IEEE/CVF Conference on Computer Vision and Pattern Recognition (CVPR)*, June 2022, pp. 4288–4298.
- [57] J. Li, J. Fan, and Z. Zhang, "Towards noiseless object contours for weakly supervised semantic segmentation," in *Proceedings of the IEEE/CVF Conference on Computer Vision and Pattern Recognition (CVPR)*, June 2022, pp. 16856–16865.



Arvi Jonnarth is an industrial Ph.D. student at Husqvarna Group, Sweden, and part of the Computer Vision Laboratory, Linköping University, Sweden. He received his M.Sc. degree in engineering physics from Uppsala University, Sweden (2018). His research interests include deep learning for computer vision and autonomous systems, with a focus on weak supervision and reinforcement learning. He is also part of the Wallenberg AI, Autonomous Systems and Software Program (WASP).



Michael Felsberg is a full professor at Linköping University, Sweden. He holds a Ph.D. degree from Kiel University, Germany (2002) and a docent degree from Linköping University (2005). His research interests include, besides visual object tracking, video object and instance segmentation, point cloud processing, and efficient machine learning techniques.



Yushan Zhang is a Ph.D. student at the Computer Vision Laboratory, Linköping University, Sweden. She is funded by the Wallenberg AI, Autonomous Systems and Software Program (WASP). She received her M.Sc. degree in optical engineering from Beijing Institute of Technology, China. Her current research interests include machine learning and computer vision.